Spectroscopic characterization of excited Ca($4s4d\delta\ ^3D_J$)RG($^3\Delta_{1,2}$) states (RG=Ar, Kr, Xe): No ''heavy-atom'' mixing of RG($nd\delta$) character into the wave functions

Allen W. K. Leung, John G. Kaup,[a] D. Bellert, John G. McCaffrey,[b] and W. H. Breckenridge

Department of Chemistry, University of Utah, Salt Lake City, Utah 84112

(Received 23 March 1999; accepted 16 April 1999)

The excited Ca($4s4d\delta\ ^3D_J$)RG[$^3\Delta_{1,2}$] states (RG=Ar, Kr, Xe) have been characterized spectroscopically by R2PI (resonance-enhanced two-photon ionization) spectroscopy. The main vibrational progressions, assigned to Ca($4s4d\delta\ ^3D_1$)RG[$^3\Delta_1$]←Ca($4s4p\pi\ ^3P_0$)·RG[$^3\Pi_{0^-}$] transitions, have weak subbands $3.7\pm0.5\ \mathrm{cm}^{-1}$ to the blue which have been assigned to analogous transitions to the $^3\Delta_2$ upper states. For CaAr and CaKr, rotational analysis has confirmed this assignment. The $^3\Delta_2/^3\Delta_1$ splitting is within experimental error the value expected if the molecular spin-orbit coupling constant is derived entirely from the Ca($4s4d\ ^3D_J$) atomic contribution. This indicates that there is no ''heavy-atom'' mixing of RG($nd\delta$) character into the wave functions of the CaRG($^3\Delta$) states. © *1999 American Institute of Physics.* [S0021-9606(99)01526-3]

I. INTRODUCTION

The van der Waals interactions of metal atoms (M) with RG atoms (RG) are one of the simplest examples of solvation at a metal site, and have received wide attention.[1] Of particular interest has been[1] the variation in bond strengths with (i) the type of outershell M-atom orbital; (ii) the alignment of that orbital with respect to the internuclear axis; and (iii) the polarizability of the RG atom. Spin-orbit (SO) effects in such complexes have also been extensively discussed with regard to mixing of orbital alignment bonding character,[1] predissociation,[1] and increases in the spin–orbit interaction by addition of ''heavy-atom'' RG character into nominally metal atom molecular orbitals.[1–8]

It has been observed in several cases[1–8] of low-lying excited ''$p\pi$'' and ''$d\pi$'' states of M*·RG (M*=excited metal atom or ion; RG=rare-gas atom) van der Waals complexes that the molecular spin-orbit coupling constant, A_{SO}, is sometimes much larger than that predicted from the *atomic* spin-orbit coupling constant of the M* excited multiplet states to which the M*·RG states correlate at large internuclear distances R. It now appears, at least for low-lying excited states M*, that such increases in A_{SO} values usually result from *direct* heavy-atom mixing of RG($np\pi$) valence character into the M*·RG wave functions at small internuclear distances R. This is consistent both with (i) the *regular* (rather than inverted) nature of the Ω multiplets, even with large increases in A_{SO}, and (ii) the increase of A_{SO} as v' decreases, consistent with greater mixing of RG($np\pi$) valence character at smaller ''effective'' distances R. The direct mixing was first demonstrated by Buenker[8,9] for the LiAr($^2\Pi$) states, and has since been confirmed by others.[10,11]

It is interesting to examine analogous cases of ''$d\delta$'' outershell M* configurations in M*($nd\delta$)·RG(Δ) excited states to see if the same kind of direct ''heavy-atom'' mixing of RG($nd\delta$) character into the M*RG(Δ) wave functions can occur. The experimental evidence to date from our laboratories on this question is indirect,[5–7] but compelling. The Mg($3s3d\ ^3D_J$) excited multiplets have a very small atomic spin-orbit coupling constant of $\sim0.02\ \mathrm{cm}^{-1}$, due to the lack of penetration of the diffuse, excited Mg($3d$) orbital to the light Mg nucleus. Consistent with no great increase in the molecular A_{SO} constant on interaction of the Mg($3d\delta$) orbital with an Ar atom, the Mg($3s3d\delta\ ^3\ ^3D_J$)·Ar[$^3\Delta$] ←Mg($3s3p\pi\ ^3P_J$)·Ar[$^3\Pi_{0^+,0^-}$] transitions could be adequately rotationally simulated[5] assuming Hund's case ''b'' character for the $^3\Delta$ upper state, e.g., that $A_{SO}<$BJ for the upperstate, consistent with A_{SO} being at most a few hundredths of a cm^{-1}. In contrast, the Mg($3s3d\delta\ ^3D_J$)·RG($^3\Delta$)←Mg($3s3p\pi\ ^3P_J$)·RG($^3\Pi_0$) transitions (RG=Kr, Xe) could be *reasonably* well-simulated[6,7] assuming simple transitions to Hund's case ''a'' $^3\Delta_1$ upperstate multiplets (P,Q,R structure only). This indicates (indirectly) that the molecular A_{SO} coupling constant has increased from hundredths of wave numbers to several wave numbers. The difference between Kr and Xe vs Ar is reasonable, given that both Kr and Xe atoms have fully occupied *valence* ($3d\delta$,$4d\delta$, respectively) filled shells of $nd\delta$ electrons (albeit inside valence $p\pi$ shells, of course), while Ar does not.

Unlike the MgAr($^3\Delta$) case, the analogous Ca($4s4d\delta\ ^3D_J$)·Ar($^3\Delta$)←Ca($4s4p\pi\ ^3P_0$)·Ar($^3\Pi_{0^-}$) rotational transitions could be well simulated[12] assuming Hund's case ''a'' character ($^3\Delta_1$) in the upperstate. Because Ca($4s4d\ ^3D_J$) has an atomic spin-orbit coupling constant of $3.7\ \mathrm{cm}^{-1}$, due to the heavier nature of the Ca atom, however, this case ''a'' behavior is reasonable, and no mixing of Ar(''$3d\delta$'') character into the wave function was necessary

[a]Present address: Department of Chemistry, Furman University, Greenville, SC 29613.

[b]Visiting Associate Professor, University of Utah, 1998; permanent address: Department of Chemistry, National University of Ireland, Maynooth, County Kildare, Ireland.

to explain the observations.[12] Here we examine new spectra of all the $Ca(4s4d\delta\,^3D_J)\cdot RG(^3\Delta_{1,2})\leftarrow Ca(4s4p\pi\,^3P_J)\cdot RG(^3\Pi_0)$ transitions (RG=Ar, Kr, Xe). In each case, weak ''subbands'' were observed $\sim 3.7\pm 0.5\,cm^{-1}$ to the blue of many of the main vibrational transitions to the $^3\Delta_1$ upper-state multiplets, and these have been assigned to case ''a'' (formally forbidden) transitions to the $^3\Delta_2$ multiplets which are weakly allowed in an intermediate (case ''a'')–(case ''b'') situation such as this one. Successful rotational simulations of both main ($^3\Delta_1$) and sub-($^3\Delta_2$) bands confirm this assignment for the CaAr and CaKr molecules. It is shown that the constant subband splittings, and the *B* constant differences for the $^3\Delta_1$, $^3\Delta_2$ pairs of bands, are exactly what is expected if the molecular A_{SO} values are derived solely from the atomic $Ca(4s4d\,^3D_J)$ SO constant. Thus, no substantial mixing of $RG(nd\delta)$ character into the $Ca^*RG(^3\Delta)$ excited state wave functions occurs. This is discussed, and a comparison is made to the analogous $Mg^*\cdot RG(^3\Delta)$ states.

II. EXPERIMENT

These experiments were carried out using an apparatus constructed for the spectroscopy of, and dynamics within, atom-$(RG)_n$, and atom-$(molecule)_n$ van der Waals complexes using either laser-induced fluorescence (LIF) or resonance two-photon ionization (R2PI) detection. The apparatus is described in more detail elsewhere.[5–7]

Briefly, calcium vapor was produced by focusing the second harmonic of a Molectron MY-32/10 Q-switched Nd:YAG laser onto a calcium target rod (1/4 in. diameter machined from Alpha/Aesar 99% pure ingot). An 800 μs pulse of gas produced by a double-solenoid pulsed valve operated at 40 psi backing pressure passed over the calcium rod coincident with the vaporization laser pulse. The gas mixtures utilized were pure Ar, 5% Kr in Ar, and 2.5% Xe in Ar. The Ca vapor/rare gas pulse then passed through a 1.8 mm orifice after having traveled 4 mm from the site of vaporization into the chamber maintained at 6×10^{-4} Torr. The beam, after passing through a 5-mm-diameter skimmer 20 cm from the source, entered the ionization region of a time-of-flight mass spectrometer at a total distance of 60 cm from the source. R2PI spectra are obtained by scanning the output of a dye laser to excite transitions from the $Ca(4s4p\pi\,^3P_J)\cdot RG(^3\Pi_{0^-},v''=0,J'')$ metastable states. Photoionization with a simultaneously pumped ionization dye laser created ions which were detected after a 1-m free-flight region. Dyes used were Coumarin 440 and 480 for resonance, Coumarin 440 for ionization.

III. RESULTS

A. Vibrational progressions

Shown in Figs. 1–3 are the vibrational main progressions, assigned to the $Ca(4s4d\delta\,^3D_1)\cdot RG[^3\Delta_1]\leftarrow Ca(4s4p\pi\,^3P_J)\cdot RG[^3\Pi_{0^-}]$ transitions, for RG=Ar, Kr, Xe. The vibrational assignments were based on isotopic splitting measurements. Shown in Fig. 4 are the isotopic band-origin shifts calculated and measured for $^{40}Ca^{82}Kr$ vs $^{40}Ca^{86}Kr$ for our assignment of v', plus those calculated for an assignment with vibrational quantum numbers greater by one. The assignment is certain, and is consistent with the first strong band in the spectrum in Fig. 2 being the (0,0) band. Shown in Fig. 5 are the measured and calculated isotopic band-origin shifts for $^{40}Ca^{129}Xe$ vs $^{40}Ca^{136}Xe$ for our assignment of v', plus those calculated for an assignment with vibrational quantum numbers greater by one. Again, the assignment is certain, and consistent with the obvious (0,0) band assignment. The analogous CaAr isotopic splitting plot has been published previously.[12] Upon close examination of the spectra, most of the bands in Figs. 1–3 are found to have weak subbands $\sim 3.7\pm 0.5\,cm^{-1}$ to the blue of the main bands, and we have assigned these subbands to transitions to the $^3\Delta_2$ multiplets. In Table I are listed all the band origins of the main bands and the subbands in Figs. 1–3.

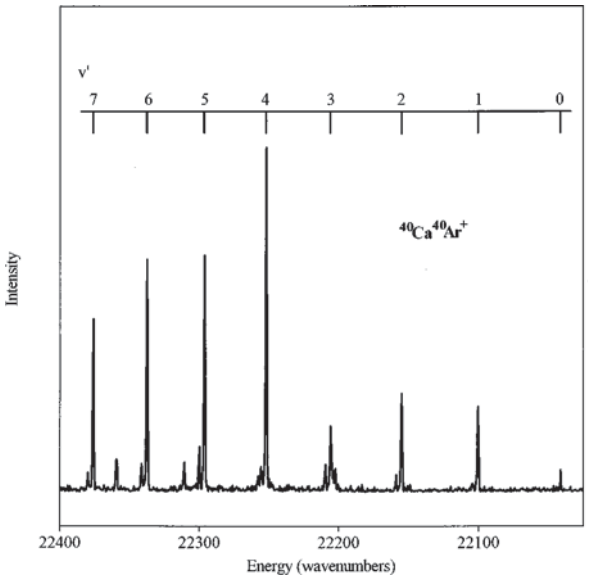

FIG. 1. The $Ca(4s4d\delta\,^3D_1)\cdot Ar[^3\Delta_1]$, $v'\leftarrow Ca(4s4p\pi\,^3P_J)\cdot Ar[^3\Pi_{0^-}]$, $v''=0$ vibrational progression.

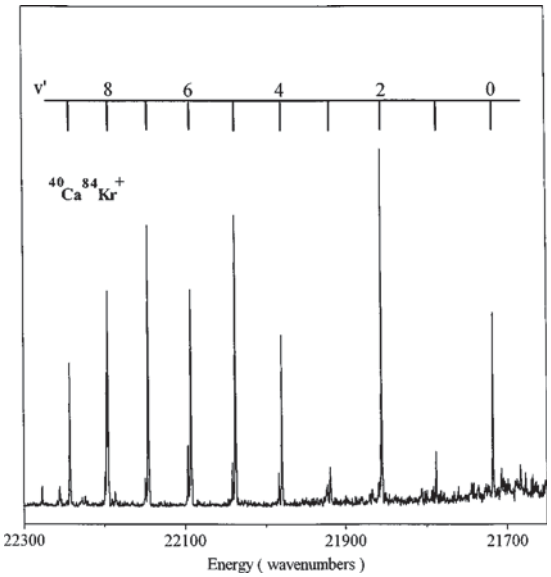

FIG. 2. The $Ca(4s4d\delta\,^3D_1)\cdot Kr[^3\Delta_1]$, $v'\leftarrow Ca(4s4p\pi\,^3P_J)\cdot Kr[^3\Pi_{0^-}]$, $v''=0$ vibrational progression.

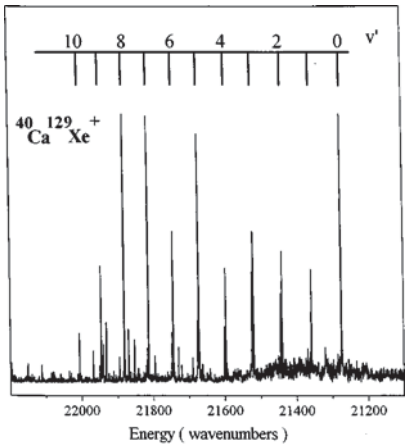

FIG. 3. The $Ca(4s4d\delta\,^3D_1)\cdot Xe[^3\Delta_1]$, $v'\leftarrow Ca(4s4p\pi\,^3P_J)\cdot Xe[^3\Pi_{0^-}]$, $v''=0$ vibrational progression.

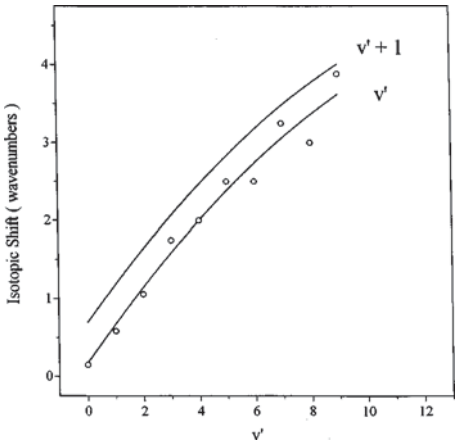

FIG. 5. A plot of the experimental isotopic shifts of the band origins of the $^{40}Ca^{129}Xe$ vs $^{40}Ca^{136}Xe$ isotopomers. Also shown are the theoretically predicted shifts for our assignment as well as an assignment with $v'+1$.

B. High-resolution rotational structure of CaAr bands

High-resolution spectra of all the CaAr bands in Fig. 1 have previously been successfully rotationally simulated as $Ca(4s4d\delta\,^3D_1)\cdot Ar[^3\Delta_1]\leftarrow Ca(4s4p\pi\,^3P_0)\cdot Ar[^3\Pi_{0^-})]$ transitions, e.g., as $(\Omega'=1)\leftarrow(\Omega''=0)$ transitions, with simple P,Q,R structure.[12] Our contention is that with the moderate $^3\Delta_1/^3\Delta_2$ splitting of only $\sim 3.7\ cm^{-1}$, the $^3\Delta$ state is somewhat intermediate between pure Hund's case ''a'' and pure Hund's case ''b,'' however, so that the ''subband'' transitions to the $^3\Delta_2$ multiplet are weakly allowed. In pure Hund's case ''b,'' the rotational energy level spacings would no longer be determined by J but by the quantum number N, and a $^3\Delta(b)\leftarrow{}^3\Pi_0$-(a) transition would have complicated $O,2P,3Q,2R,S$ type branch structure. But since the $^3\Delta_{1,2}$ states are actually closer to case ''a,'' so that Ω is still an approximately good quantum number, we have attempted to simulate a new high-resolution $^3\Delta_2\leftarrow{}^3\Pi_0$-subband spectrum assuming a $(\Omega'=1)\leftarrow(\Omega''=0)$ transition, but leaving out all transitions for which ΔJ is not 0 or ± 1. The $R(0)$, $P(2)$, and $Q(1)$ branch intensities, included in the ''main-band'' simulations, were thus set to zero for the subband simulations. [This is *equivalent* to a $(\Omega'=2)\leftarrow(\Omega''=1)$ transition.]

Shown in Fig. 6 is the experimental (5,0) $^3\Delta_2\leftarrow{}^3\Pi_0$- subband, and the successful computer simulation of the rotational structure. The band contours near the origin were less well simulated if the $R(0)$ and $Q(1)$ branches were included rather than left out. This is consistent with, but is not definitive proof of, the band assignment. However, the substantial difference in the observed B_5' rotational constant for the subband versus the main-band *is*. The best-fit value of B_5' for the simulation in Fig. 6 is $0.0711\ cm^{-1}$, while B_5' for the main band was determined to be $0.0686\ cm^{-1}$ (the known[12,13] value of $B_0''=0.0555\,cm^{-1}$ was used in both simulations, and the uncertainty in the ΔB values is small). When $A\gg B_v$, the dependence on Λ and Σ of the ''effective'' B constants of case ''a'' triplet states is given

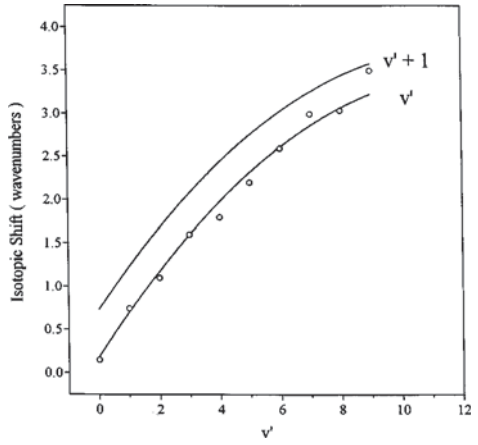

FIG. 4. A plot of the experimental isotopic shifts of the band origins of the $^{40}Ca^{82}Kr$ vs $^{40}Ca^{86}Kr$ isotopomers. Also shown are the theoretically predicted shifts for our assignment as well as an assignment with $v'+1$.

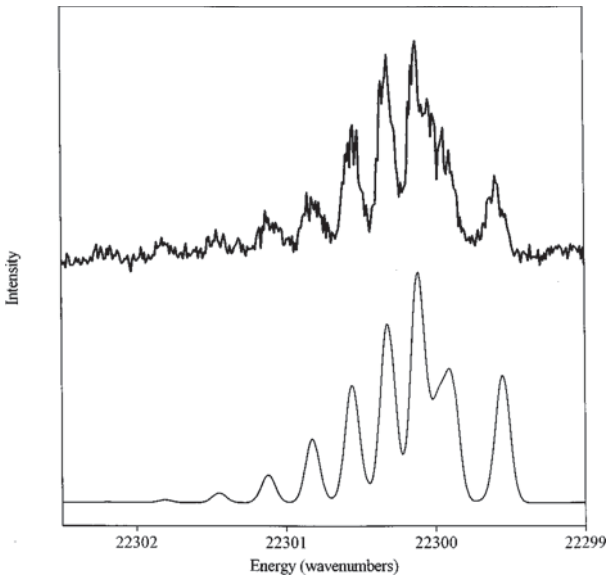

FIG. 6. High-resolution spectrum, and computer simulation, of the (5,0) subband, $CaAr(^3\Delta_2)$; simulation parameters: $T=1.0$ K; laser linewidth: $0.11\ cm^{-1}$; $B_0''=0.0555\,cm^{-1}$; $B_5'=0.0711\,cm^{-1}$; saturated line strengths; intensities of $R(0)$, $Q(1)$, and $P(2)$ transitions were set to zero.

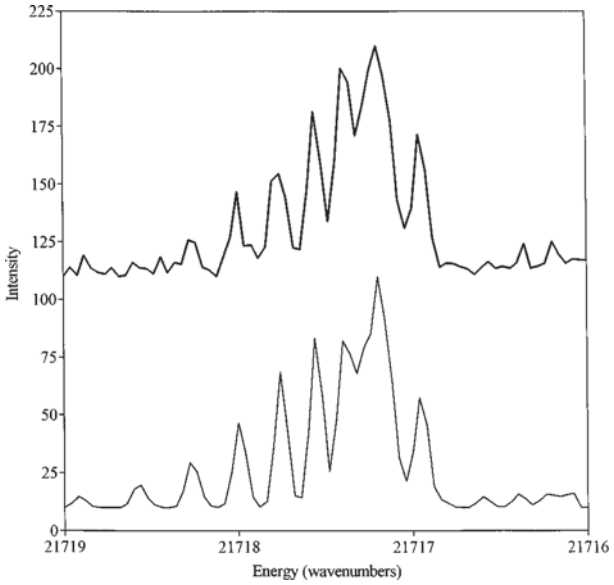

FIG. 7. High-resolution spectrum, and computer simulation, of the (0,0) band, CaKr($^3\Delta_1$); simulation parameters: $T=1.0$ K; laser linewidth: 0.08 cm^{-1}; $B_0''=0.0430\,cm^{-1}$; $B_0'=0.0586\,cm^{-1}$; $0^+/0^-$ energy separation: $+1.16\,cm^{-1}$; $0^+/0^-$ population ratio: 0.08; saturated line strengths.

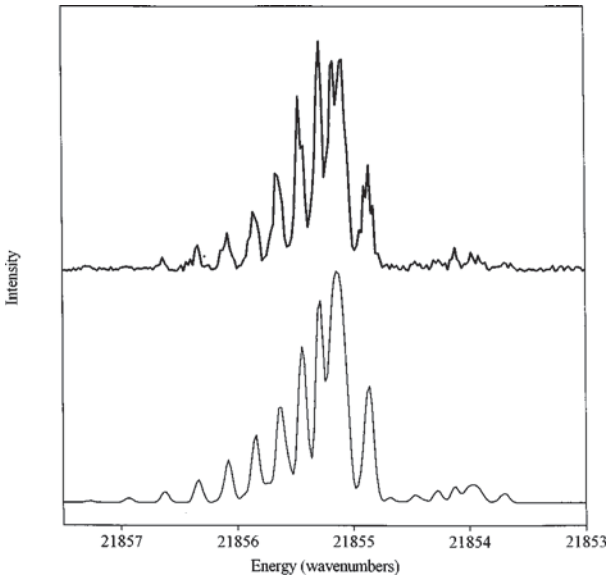

FIG. 8. High-resolution spectrum, and computer simulation, of the (2,0) band, CaKr($^3\Delta_1$); simulation parameters: same as Fig. 7, except $B_2'=0.0555\,cm^{-1}$.

approximately[14] by: $B_{\text{eff}}=B_v[1+(2B_v\Sigma/A\Lambda)]$, where A is the molecular SO coupling constant, which here is equal to $\sim 3.7/2=1.85\,cm^{-1}$ ($T_e=T_0+A\Lambda\Sigma$; see Sec. IV).[15] For the $^3\Delta_2$ state, where $\Sigma=0$, $B'_{\text{eff}(5)}=0.0711\,cm^{-1}=B_5'$ (true). For the $^3\Delta_1$ state, where $\Sigma=-1$, $B'_{\text{eff}(5)}=0.0711[1-2(0.0711)/(1.85)(2)]=0.0684\,cm^{-1}$, is essentially the same as the 0.0686 cm^{-1} value determined experimentally, within experimental error. This shows that our assignment of the subbands to $^3\Delta_2$ multiplets is correct for the CaAr case.

C. High-resolution rotational structure of the CaKr bands

The rotational structures of several of the main bands were obtained in high resolution and were successfully simulated assuming the same $^3\Delta_1\leftarrow{}^3\Pi_{0^-}$ band structure (a small population of the $^3\Pi_{0^+}$ lower state ($10\pm5\%$) is known to be present in the CaKr case, ~ 1.16 cm^{-1} higher in energy than the $^3\Pi_{0^-}$ state).[13] Shown in Figs. 7–10 are experimental spectra and computer simulations of several bands. We have also been able (with difficulty) to record a subband at sufficient resolution for computer simulation, the (4,0) subband, shown in Fig. 11 along with the ''best-fit'' simulation (see above section on CaAr spectra). A similar analysis to that explained above results in $B_4'(^3\Delta_2)=0.0545\,cm^{-1}$, leading to a *prediction* of $B_4'(^3\Delta_1)=0.0526\,cm^{-1}$ compared to the observed value of $B_4'(^3\Delta_1)=0.0529\,cm^{-1}$. This shows that our assignment of the upperstate of the subbands to the $^3\Delta_2$ multiplet is also correct for the CaKr case.

Sufficient rotational resolution of neither the CaXe main bands, nor a subband, was achieved, so the CaXe assignments in Table I must be formally regarded as tentative at this stage (but probably correct; see Sec. IV).

D. Spectroscopic constants

From linear Birger–Sponer plots, ω_e and $\omega_e x_e$ upperstate values were determined, and $D_e[=(\omega_e^2/4\omega_e x_e)]$ values were estimated. However, more accurate values of D_0 (and D_e) can be obtained, we believe, from the estimated D_0 values for the more weakly bound lower $^3\Pi_{0^-}$ states, and a thermochemical cycle:

$$D_0(^3\Delta_1)=D_0(^3\Pi_{0^-})+E(^3D_1)-E(^3P_0)-\nu_{0,0}.$$

Both values are listed in Table II.

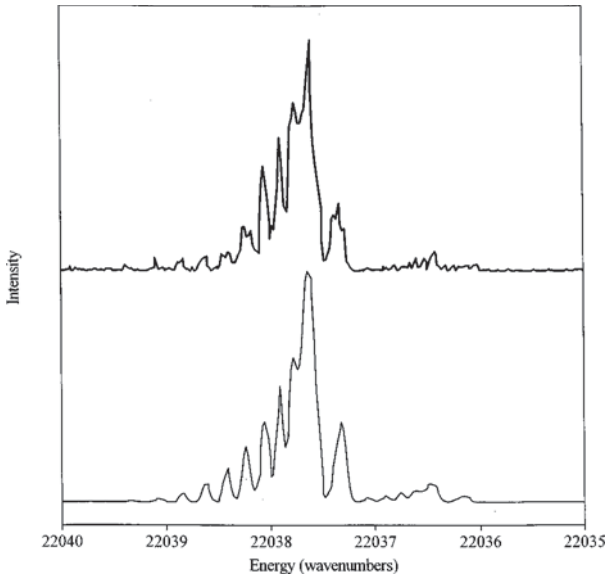

FIG. 9. High-resolution spectrum, and computer simulation, of the (5,0) band, CaKr($^3\Delta_1$); simulation parameters: same as Fig. 7, except $B_5'=0.0513\,cm^{-1}$.

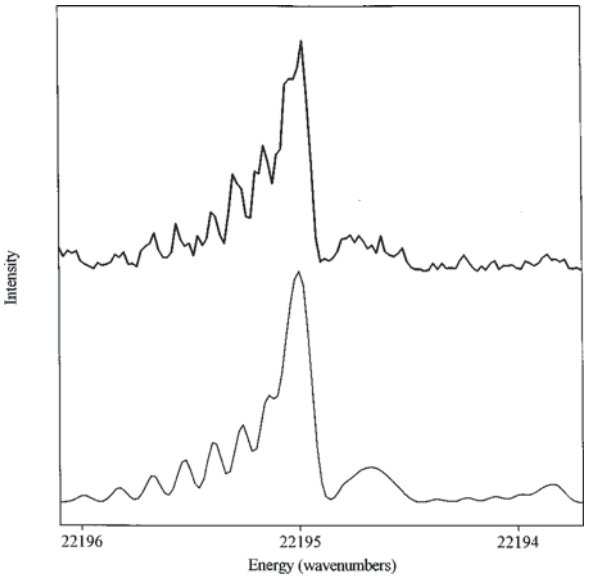

FIG. 10. High-resolution spectrum, and computer simulation, of the (8,0) band, CaKr($^3\Delta_1$); simulation parameters: same as Fig. 7, except $B_8' = 0.0479\ \mathrm{cm}^{-1}$.

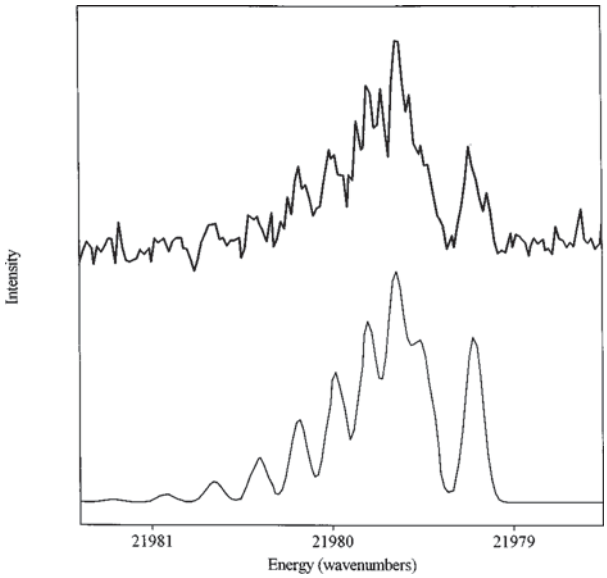

FIG. 11. High-resolution spectrum, and computer simulation, of the (4,0) subband, CaKr($^3\Delta_2$); simulation parameters: $T = 0.8$ K; laser linewidth$= 0.11\ \mathrm{cm}^{-1}$; $B_0'' = 0.0430\ \mathrm{cm}^{-1}$; $B_4' = 0.0545\ \mathrm{cm}^{-1}$; saturated line strengths; intensities of $R(0)$, $Q(1)$, and $P(2)$ transitions were set to zero.

From the variation of $B_{v'}$ with v', the B_e' and α_e' values were determined, from which R_e' and R_0' bond lengths were computed for CaAr and CaKr. This information is listed in Table II.

IV. DISCUSSION

A. No mixing of RG($nd\delta$) character into the Ca($4s4d\delta\,^3D_J$)·RG($^3\Delta_{1,2}$) wave functions

The atomic Ca($4s4d\,^3D_J$) spin-orbit coupling constant ζ_δ is 3.7 cm^{-1} $[(E_{^3D_3} - E_{^3D_1})(2/5)]$.[16] Since[16] $\langle {}^3\Delta_1 | H_{\mathrm{SO}} | {}^3\Delta_1 \rangle = \langle \delta^+\beta | a_\delta \cdot \hat{\ell}_z \cdot \hat{s}_z | \delta^+\beta \rangle$, and $\hat{\ell}_z|\delta^+\rangle = +2\hbar|\delta^+\rangle$ and $\hat{s}_z|\beta\rangle = -\hbar/2|\beta\rangle$, this is equal to $\langle \delta^+\beta | a_\delta (2\hbar)(-\hbar/2) | \delta^+\beta \rangle$. Thus, $E_{^3\Delta_1} = -a_\delta(\hbar)^2 = -\zeta_\delta$ for the $^3\Delta_1$ state. But since[15] $T_e = T_0 + A\Lambda\Sigma$, $E_{^3\Delta_1} = E_{^3\Delta_2} + A(2)(-1)$, so $E_{^3\Delta_2} - E_{^3\Delta_1} = 2A_\delta = 3.7\ \mathrm{cm}^{-1} = \zeta_\delta$; and $A_\delta = \zeta_\delta/2 = 1.85\ \mathrm{cm}^{-1}$. Thus, the observed $^3\Delta_2/{}^3\Delta_1$ energy splitting of $3.7 \pm 0.5\ \mathrm{cm}^{-1}$ is exactly what is expected from the asymptotic Ca(^3D_J) SO coupling constant, showing that any mixing of RG($nd\delta$) character into the Ca($4s4d\delta\,^3D_J$)·RG($^3\Delta_{1,2}$) wave functions is insufficient to change the A_δ value from the expected $1.85\ \mathrm{cm}^{-1}$.

B. Comparison with the analogous Mg($3s3d\delta\,^3D_J$)·RG states

As discussed in Sec. I, the apparent case ''a'' nature[6,7] of the $3d\delta\,^3\Delta$ states of MgKr and MgXe appears to indicate that there is a mixing of Kr($3d\delta$) and Xe($4d\delta$) character sufficient to increase the effective SO coupling from ~ 0.02 cm^{-1} to as much as several cm^{-1}. A careful reexamination of the MgRG($^3\Delta$) spectra showed no evidence of subbands, however, so molecular A_{SO} coupling constants have not been directly measured for these states.

It is possible that the interaction (and thus mixing) of the Mg($3s3d\delta\,^3D$) orbital with the Kr($3d\delta$) and Xe($4d\delta$) or-

TABLE I. Band origins for the $^3\Delta_{1,2} \leftarrow {}^3\Pi_{0^-}$ transitions ($+20\,000\ \mathrm{cm}^{-1}$) (taken mostly from maxima in low-resolution scans).

	^{40}Ca^{40}Ar		^{40}Ca^{84}Kr		^{40}Ca^{129}Xe	
	$^3\Delta_1$	$^3\Delta_2$	$^3\Delta_1$	$^3\Delta_2$	$^3\Delta_1$	$^3\Delta_2$
(0,0)	2041.1	⋯	1717.5	⋯	1274.0	⋯
(1,0)	2099.9	2103.9	1788.0	1792.0	1358.1	⋯
(2,0)	2154.4	2158.4	1855.0	1858.8	1400.1	1404.1
(3,0)	2205.6	2209.1	1919.5	1922.5	1519.8	1523.8
(4,0)	2251.7	2255.7	1975.8	1979.5	1596.8	1600.3
(5,0)	2295.9	2299.4	2037.50	2041.5	1671.3	1674.3
(6,0)	2337.0	2341.0	2092.5	2096.3	1742.8	1746.3
(7,0)	2375.7	2379.7	2145.0	2148.8	1812.8	1815.8
(8,0)	2411.7	2415.7	2195.0	⋯	1879.8	⋯
(9,0)	⋯	⋯	2242.5	⋯	1945.2	⋯
$E_{^3\Delta_2} - E_{^3\Delta_1}$ (cm^{-1})	3.9 ± 0.5		3.7 ± 0.5		3.6 ± 0.5	

TABLE II. Spectroscopic constants for the Ca($4s4p\pi\,^3P_J$)·RG[$^3\Pi_{0^-}$] and Ca($4s4d\delta\,^3D_J$)·RG($^3\Delta_1$) states.

	^{40}Ca^{40}Ar		^{40}Ca^{84}Kr		^{40}Ca^{129}Xe	
	$^3\Pi_{0^-}$	$^3\Delta_1$[a]	$^3\Pi_{0^-}$	$^3\Delta_1$	$^3\Pi_{0^-}$	$^3\Delta_1$
$\nu_{0,0}$	···	22041.1	···	21717.5	···	21274.0
ω_e		60.5±1.0	···	72.58±0.29		86.42±0.11
$\omega_e x_e$		1.61±0.11		1.439±0.028		1.195±0.011
B_o	0.0555±0.0030[a,b]	0.0811±0.0030	0.0430±0.0023[b]	0.05860±0.0023	0.0300±0.0022[b]	···
B_e	···	0.0822±0.0030[d]	···	0.05901±0.0023[e]	···	···
α_e	···	0.0025±0.0001	···	0.001 34±0.000 062	···	···
R_o	3.90±0.10[a,b]	3.23±0.06	3.81±0.10[b]	3.26±0.06	4.28±0.15[b]	···
R_e	···	3.20±0.06[d]	···	3.25±0.06[e]	···	···
D_o	60±50[c]	609±50	120±60[c]	993±60	300±80[c]	1616±80
		(538)		(879)		(1520)
D_e		639±50	···	1029±60		1659±80
		(568)		(915)		(1562)

[a]Reference 12.
[b]Reference 13.
[c]Reference 17.
[d]''True'' B_e, of the $^3\Delta_2$ state, is 0.0859 cm^{-1}, R_e=3.13 Å.
[e]''True'' B_e, of the $^3\Delta_2$ state, is 0.0609 cm^{-1}, R_e=3.20 Å.

bitals is much stronger than for the Ca($4s4d\delta\,^3D$) case, increasing the A_{SO} to >4 cm^{-1}, and thus perhaps *decreasing* the subband intensities below detection limits (purer case ''a'' character). The bond strengths of the CaKr($^3\Delta_1$) and CaXe($^3\Delta_1$) states (see Table III) are much less,[5–7,12] and the bond lengths much longer,[5–7,12] than for the MgKr($3d\delta\,^3\Delta$) and MgXe($3d\delta\,^3\Delta$) analog, consistent with this idea.

C. van der Waals bonding in ''valence'' M($nsnd\delta\,^3D_J$)·RG($^3\Delta$) states

Shown in Table III are D_e, ω_e, and R_e values for several states of CaRG neutrals and ions. As can be seen the excited CaRG($^3\Delta$) states are quite strongly bound, approaching even the bond strengths of the Ca$^+$·RG ions. This can be rationalized by the fact that the RG atoms approach along the nodal axis of the excited, diffuse Ca($4d\delta$) orbital. Thus, repulsion with RG outershell electron density is minimized, and the RG atoms see something approximating the ''bare'' Ca$^+$($4s$) ion core at small R. The bond energies are thus only slightly less than the Ca$^+$($4s$)·RG ion bond energies. This is in contrast to the lower-state Ca($4s4p\pi\,^3P_J$)·RG($^3\Pi_0$) bond energies, where the Ca($4p\pi$) orbital is much lower in energy [~15 000 cm^{-1} vs ~38 000 cm^{-1} for the Ca($4d\delta$) orbital] and is thus less diffuse, leading to more repulsion and lower relative bond energies, even though the RG atom also approaches along the Ca($4p\pi$) nodal axis. (The $^3\Pi_0$–D_0 values are also substantially further reduced due to the large (A_{SO}=211 cm^{-1}) spin-orbit-induced σ/π ''mixed'' character of the $\Omega=0^-$ multiplet.)

TABLE III. Bond energies, vibrational frequencies, and bond lengths of several CaRG and Ca$^+$RG states.

	D_o (cm^{-1})	ω_e (cm^{-1})	R_o (Å)
CaAr($4s4p\pi\,^3\Pi_{0^-}$)[a,b,c]	60±50	···	3.9±0.1
CaAr($4s5s\,^3\Sigma^+$)[b]	564±50	81	3.13±0.06
CaAr($4s4d\delta\,^3\Delta_1$)[a]	609±50	61	3.23±0.06
Ca$^+$Ar($4s\,^2\Sigma^+$)	775±50[c]	69[d]	···
CaKr($4s4p\pi\,^3\Pi_{0^-}$)[b,c]	120±60	···	3.8±0.1
CaKr($4s5s\,^3\Sigma^+$)[b]	980±60	87	3.37±0.08
CaKr($4s4d\delta\,^3\Delta_1$)[e]	993±60	73	3.26±0.06
Ca$^+$Kr($4s\,^2\Sigma^+$)	1244±60[c]	77[d]	···
CaXe($4s4p\pi\,^3\Pi_{0^-}$)[b,c]	300±80	···	4.3±0.2
CaXe($4s5s\,^3\Sigma^+$)[b]	1705±80	106	3.59±0.12
CaXe($4s4d\delta\,^3\Delta_1$)[e]	1616±80	86	···
Ca$^+$Xe($4s\,^2\Sigma^+$)	1811±80[c]	86[d]	···

[a]Reference 12.
[b]Reference 13.
[c]Reference 17.
[d]Reference 3.
[e]This work.

The percent of the bond energies of the Ca($4d\delta\,^3\Delta$)·RG states versus those of the respective Ca$^+$RG ions also increases (73%, 79%, 89%) in the order RG=Ar, Kr, Xe. A similar trend is observed for the first Ca($5s\,^3\Sigma^+$) Rydberg states (79%, 80%, 94%), where it is thought that the RG atom can ''penetrate'' beneath the outer Ca($5s$) lobes of electron density and also feel an attraction approaching that of the Ca$^+$RG ions at small R.

The fundamental vibrational frequencies ω_e of the Ca($4d\delta\,^3\Delta$)·RG states are also similar to (usually slightly lower than) those of the analogous Ca$^+$·RG ions. In contrast, the Ca($5s\,^3\Sigma^+$) Rydberg states have much higher relative values of ω_e, and this is thought to be due to the fact that at large R, as the RG atoms attempt to penetrate the Ca($5s$) outerlobe, there is either a maximum or a ''flatness'' in the potential curve, so that when the ''Ca$^+$RG'' attraction suddenly sets in at smaller R, the potential curves are narrower, leading to higher vibrational frequencies (but similar D_0 and R_0 values).

ACKNOWLEDGMENTS

The authors are grateful for funding of this research by the National Science Foundation and the Petroleum Research Fund. One of us (W.H.B) acknowledges useful conversations regarding spin-orbit coupling with Professor Michael Morse.

[1] W. H. Breckenridge, C. Jouvet, and B. Soep, in *Advances in Metal and Semiconductor Clusters*, edited by M. Duncan (JAI, Greenwich, 1995), Vol. 3.
[2] J. S. Pilgrim, C. S. Yeh, K. R. Berry, and M. A. Duncan, J. Chem. Phys. **100**, 7945 (1994).
[3] S. H. Pullins, C. T. Scurlock, J. E. Reddic, and M. A. Duncan, J. Chem. Phys. **104**, 7518 (1996).
[4] J. E. Reddic and M. A. Duncan, J. Chem. Phys. (in press).
[5] S. Massick and W. H. Breckenridge, J. Chem. Phys. **105**, 9719 (1996).
[6] J. G. Kaup and W. H. Breckenridge, J. Chem. Phys. **107**, 6005 (1997).
[7] J. G. Kaup and W. H. Breckenridge, J. Chem. Phys. **107**, 6014 (1997).
[8] J.-P. Gu, G. Hirsch, R. J. Buenker, I. D. Petsalakis, G. Theodorakopoulos, and M. B. Huang, Chem. Phys. Lett. **230**, 473 (1994).
[9] R. J. Buenker (private communication).
[10] S. Matsila and R. M. Pitzer, J. Phys. Chem. A **102**, 1652 (1998).
[11] K. Sohlberg and D. R. Yarkony, J. Chem. Phys. **107**, 7690 (1997).
[12] J. G. Kaup and W. H. Breckenridge, J. Chem. Phys. **107**, 5676 (1997).
[13] J. G. Kaup and W. H. Breckenridge, J. Chem. Phys. **107**, 5283 (1997).
[14] G. Herzberg, *Spectra of Diatomic Molecules* (Van Nostrand Reinhold, New York, 1950), p. 235.
[15] G. Herzberg, *Spectra of Diatomic Molecules* (Van Nostrand Reinhold, New York, 1950), p. 215.
[16] H. LeFebvre-Brion and R. W. Field, *Perturbations in the Spectra of Diatomic Molecules* (Academic, Orlando, 1986).
[17] J. G. Kaup and W. H. Breckenridge, J. Chem. Phys. **107**, 4451 (1997).